Probing the Origins of Increased Activity of the E22Q "Dutch" Mutant Alzheimer's β-Amyloid Peptide

Francesca Massi and John E. Straub

Department of Chemistry, Boston University, Boston, Massachusetts 02215 USA

ABSTRACT   The amyloid peptide congener Aβ(10–35)-NH$_2$ is simulated in an aqueous environment in both the wild type (WT) and E22Q "Dutch" mutant forms. The origin of the noted increase in deposition activity resulting from the Dutch mutation is investigated. Multiple nanosecond time scale molecular dynamics trajectories were performed and analyzed using a variety of measures of the peptide's average structure, hydration, conformational fluctuations, and dynamics. The results of the study support the conclusions that 1) the E22Q mutant and WT peptide are both stable in "collapsed coil" conformations consistent with the WT structure of Zhang et al. (2000, *J. Struct. Biol.* 130:130–141); 2) the E22Q peptide is more flexible in solution, supporting early claims that its equilibrium structural fluctuations are larger than those of the WT peptide; and 3) the local E22Q mutation leads to a change in the first solvation layer in the region of the peptide's "hydrophobic patch," resulting in a more hydrophobic solvation of the mutant peptide. The simulation results support the view that the noted increase in activity due to the Dutch mutation results from an enhancement of the desolvation process that is an essential step in the aggregation of the peptide.

BACKGROUND

The β-amyloid hypothesis, championed by Selkoe (1994, 1997) and others, is the most studied and best developed theory for one of the underlying causes of Alzheimer's disease. A growing number of experimental studies of the structure of solvated peptide and fibrils, and the activity of the peptide in the process of fibril growth, are beginning to define the fundamentals of a mechanism of amyloid fibrillogenesis and fibril elongation.

A number of proposals (Zagorski and Barrow, 1992; Talafous et al., 1994) have been put forward regarding the activity of the Aβ-peptide and its sequence dependence. An early proposal was based on the paradigm of an α→β transition, where the peptide, which was assumed to be predominately α-helical, underwent a solution phase conformational transition to an activated form of the peptide. This activated form was characterized by backbone geometry that was largely β-sheet or strand and consistent with the predominately β-form of the fibril aggregates.

That initial proposal is still seriously considered by some (Marcinowski et al., 1998; Shao et al., 1998). However, there is a growing body of evidence that argues against it. Most notably, a solution phase NMR structure of a Aβ(10–35)-peptide congener has been determined by Lee and coworkers (Zhang et al., 2000). The structure, which was described as a "collapsed coil" (cc) and characterized by a central hydrophobic cluster and a robust adjacent turn region, clearly demonstrates that the peptide lacks α-helical character as a monomer in aqueous solution. Subsequent

multiple nanosecond molecular dynamics calculations of the fully solvated Aβ(10–35)-peptide congener found that the peptide exhibited stable fluctuations about the characteristic collapsed coil structure (Massi et al., 2001). Comparison with experimental measures of structure, fluctuations, and dynamics derived from NMR and quasielastic light scattering experiments, including NMR amide bond order parameters, peptide diffusion constants, and the radius of gyration, indicated that the simulation model captured not only the dominant features of the stable peptide fold but the range of fluctuations in the less structured C- and N-terminal regions of the peptide.

Although these experimental and computational data argue against the significance of an α→β transition in the solution phase monomeric peptide, it is possible that a cc→β transition could be essential to the peptide's activity. Experimental studies of Aβ-peptide fibril elongation by Teplow and coworkers (Kusumoto et al., 1998) and deposition by Maggio and coworkers (Esler et al., 1996, 2000b), have recently been analyzed in terms of an "energy landscape mechanism" for Aβ-peptide fibril elongation by Massi and Straub (2001). Our proposed mechanism consists of two principal channels: 1) a prion-like channel where the monomeric peptide undergoes a fluctuation to an activated β-peptide state followed by fast addition to the existing β-fibril, and 2) a two-step mechanism of nonspecific adsorption of the collapsed coil peptide on the fibril surface followed by reorganization to well-formed β-fibril. As such, it unifies the proposed mechanisms of a crucial cc→β conformational transition in the monomeric peptide with the adsorption/reorganization pathway first proposed by Teplow and coworkers (Kusumoto et al., 1998) and expanded on by Maggio and coworkers (Esler et al., 2000b). Experimental evidence suggests that for the activity of the wild type Aβ(10–35)-peptide, the second channel—a two-step process of adsorption and reorganization—may pre-

dominate. However, the proposed mechanism of Massi and Straub is inclusive of both pathways, and the associated kinetics gives an excellent fit with experimental data for rates of deposition and fibril elongation (Massi and Straub, 2001).

An important goal of research on Aβ-peptide aggregation is to understand the role of sequence in the peptide's activity, where it is known that sequence can play a crucial role. Two particular naturally occurring mutant forms of the wild type Aβ-peptide, the E22Q "Dutch" mutant and the E22K "Italian" mutant, have been the focus of structural and activity studies (Miravalle et al., 2000; Melchor et al., 2000). To date, it is well understood that the E22Q mutant shows enhanced activity (as measured by the rate of deposition or fibril elongation) relative to the wild type (WT) peptide for both the 1–42 Aβ-peptide and the Aβ(10–35)-peptide congener (Miravalle et al., 2000; Esler et al., 2000a). The exact nature of the structure of the monomeric E22Q mutant peptide in aqueous solution however, remains controversial.

There is, to date, no NMR-derived structure of the E22Q mutant peptide analogous to the structure of the WT Aβ(10–35)-peptide congener. However, NMR measurements of H_α proton chemical shifts for the WT and E22Q mutant Aβ(10–35)-peptides are consistent with a structure of the E22Q mutant that is indistinguishable from the known cc structure of the WT peptide (Zhang, 1999).

In a related study, the rate of peptide deposition was measured for the Aβ(10–35)-peptide congener (Esler et al., 2000a). A simple and approximate Arrhenius rate theory model was used to derive the activation enthalpy and entropy for the deposition rate constants of the WT and the E22Q mutant forms of the peptide (where the mutant peptide was found to deposit at a rate 215% faster than the WT peptide). The authors attributed the difference between the activity of the WT and E22Q peptides to a difference in the entropy of activation, implying that the mutant peptide was characterized by a looser, entropically stabilized transition state structure relative to that of the WT peptide (Esler et al., 2000a).

In a study of Austen and coworkers (Sian et al., 2000), it was found that Aβ(1–40)E22Q peptide formed oligomers and fibrils more rapidly than the WT peptide. Using circular dichroism (CD) spectroscopy, they observed that the rate of change from mainly random coil to β-sheet was more than one order of magnitude higher in the E22Q than in the WT. The rates of conversion from random coil to β-sheet in the WT and E22Q mutant peptides, derived from CD measurements, were an order of magnitude lower than the rate of formation of low-molecular-mass oligomers (detected by ELISA and gel filtration). The study concluded that the Aβ-peptide aggregates into an irregular structure and subsequently undergoes a slower conformational transition into aggregates of β-sheets. Such a pathway is consistent with

the second channel of the mechanism of Massi and Straub (2001).

However, there is also evidence that the E22Q peptide has a propensity for the formation of β-structure in solution. One study, performed by Selkoe and coworkers (Watson et al., 1997), explored the binding of heparin to solutions of WT and E22Q mutant Aβ-peptide. Heparin binds to fibrillar (and not to nonfibrillar) Aβ-peptide. However, the underlying cause of the specificity of binding is not understood. Peptide was neutralized in a 1-mM aqueous solution and incubated for 48 h at 4°C and then lyophilized. It was found that the E22Q mutant peptide assumed conformations to which heparin would bind more readily than did the WT peptide. In fact, the affinity of heparin binding to the E22Q mutant peptide was similar to the affinity for binding of heparin to preformed β-fibrils. The conclusion was that the water-aggregated E22Q mutant peptide adopted structures similar to those found in fibrils with substantial β-pleated sheet conformation (Watson et al., 1997).

An experimental study by Miravalle et al. (2000) using CD and Fourier transform infrared spectroscopy measurements found that, although the WT and the E22K peptide were largely of the random coil conformation in solution, the E22Q peptide assumed a β-sheet conformation. The study explored the time dependence of peptide aggregation by CD and showed that, for their sample preparations, the WT, E22K, and E22Q peptide converted to β-structure over a period of hours. However, although CD spectra of the WT and E22K peptide samples indicated that, at the earliest times, the peptide was in a random coil conformation, the E22Q peptide sample showed the clear signs of β-structure. This observation could be used to support the hypothesis that the E22Q mutant peptide may form an "activated" β-form of the monomeric peptide more readily than the WT peptide (Miravalle et al., 2000). Such a mechanism would be consistent with the first channel of the mechanism of Massi and Straub. However, the results in the case of the E22Q mutant peptide could also be due to the presence of peptide aggregates from the earliest stages of the CD measurements.

A possible explanation for these discrepancies lies in the sample preparation. The NMR studies of Lee and coworkers (Zhang et al., 2000), which included WT and E22Q peptides samples at 250 μM and higher concentration, was based on a careful preparation of a stable sample of dissolved, monomeric peptide. As has been noted, the careful preparation of samples, through extensive ultracentrifugation to remove "seeds" that might nucleate aggregates, can result in samples of monomeric peptide that are stable for months at a time. Less rigorous sample-preparation protocols may result in artifacts due to incomplete dissolution.

In this computational study, we explore the hypothesis that the E22Q mutation leads to a monomeric peptide that has a higher propensity, relative to the WT peptide, for undergoing conformational fluctuations to an activated
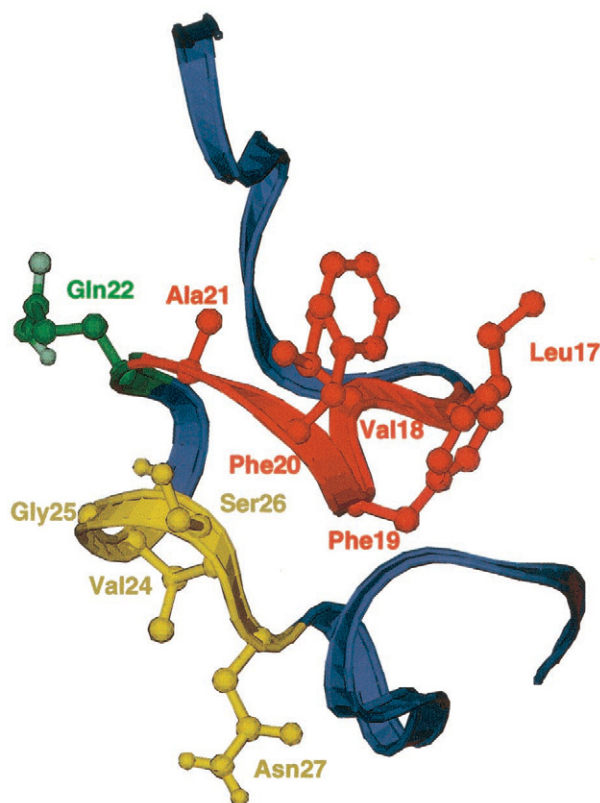
FIGURE 1 The E22Q mutant form of the congener amyloid β(10–35)-NH$_2$ peptide is depicted. From the N-terminus, the groups are Tyr[10]-Glu[11]-Val[12]-His[13]-His[14]-Gln[15]-Lys[16] (blue/gray), Leu[17]-Val[18]-Phe[19]-Phe[20]-Ala[21] (red), Glu[22] (green), Asp[23] (blue/gray), Val[24]-Gly[25]-Ser[26]-Asn[27] (yellow), Lys[28]-Gly[29]-Ala[30]-Ile[32]-Gly[33]-Leu[34]-Met[35] (blue/gray).

β-form of the peptide. Multiple nanosecond time scale molecular dynamics trajectories were performed and analyzed using a variety of measures of the peptide's average structure, hydration, conformational fluctuations, and dynamics. The results of the study support the following conclusions. 1) The E22Q mutant and WT peptide are both stable in cc conformations consistent with the WT structure of Lee and coworkers (Zhang et al., 2000). 2) The E22Q peptide is more flexible in solution, consistent with early claims that its equilibrium structural fluctuations were larger than those of the WT peptide. 3) The local E22Q mutation leads to a change in peptide hydration and the structure of the first solvation layer in the region of the peptide's "hydrophobic patch." Our concluding discussion includes speculation on how these observations lead to a consistent picture of the observed increased activity of the E22Q mutant relative to the WT peptide.

METHODS

The starting point for our simulations of the wild type β(10–35)-NH$_2$ peptide and the E22Q mutant peptide was the WT nuclear magnetic resonance (NMR) solution structure of Lee and coworkers (Zhang et al.,

2000) derived from distance geometry calculations using NMR-derived NOE restraints. The initial structure of the E22Q mutant was derived from the WT structure by mutating residue 22. The E22Q Dutch mutant peptide congener is depicted in Fig. 1. The colored regions are Tyr[10]-Glu[11]-Val[12]-His[13]-His[14]-Gln[15]-Lys[16] (blue/gray), Leu[17]-Val[18]-Phe[19]-Phe[20]-Ala[21] (red), Glu[22]/Gln[22] (green), Asp[23] (blue/gray), Val[24]-Gly[25]-Ser[26]-Asn[27] (yellow), Lys[28]-Gly[29]-Ala[30]-Ile[31]-Ile[32]-Gly[33]-Leu[34]-Met[35] (blue/gray). The dominant structural motifs in the peptide are the hydrophobic cluster LVFFA 17–21 segment (red), the turn 24–27 VGSN segment (yellow), and the glutamine residue Q22 that is positioned at the interface between the hydrophobic cluster and turn regions.

For the fully solvated WT and mutant peptide, four independent 1-ns trajectories were simulated. Each trajectory originated from one of a set of four initial peptide structures that were chosen from two families of conformers characterized by variations in their C-terminal regions. The initial structures resulted from the work of Lee and coworkers who used a combination of distance geometry refinement and molecular dynamics annealing/minimization procedures using experimentally derived NOE restraints. Further details of the refinement have been published elsewhere (Lee et al., 1995; Zhang, 1999; Zhang et al., 2000; Massi et al., 2001).

In the remainder of this section, we describe the simulation model used in our study. The standard methods used to characterize the peptide's structure and fluctuations include amide bond vector order parameters, residue fluctuation matrix, rates of self-diffusion, measures of backbone fluctuation, and ordering of water molecules in the first solvation shell. A description of many elements of this analysis protocol has been previously presented (Massi et al., 2001).

Simulation model of the WT peptide congener in aqueous solution

For the simulations of the wild-type and mutant peptides, the solute was centered in a rhombic dodecahedron cell that was carved from a cubic box of 50 Å on a side and then filled with 2113 water molecules. Because periodic boundary conditions were applied to avoid edge effects, this corresponds to a 31-mM concentration of peptide. The energetics of the Aβ peptide in water was simulated using the version 22 potential energy function of the CHARMM program (Mackerell et al., 1998). The potential energy cut-off distance for the nonbonded interactions was 12.0 Å. Ewald summation was used to evaluate the electrostatic interactions. SHAKE was used to constrain bonds involving hydrogen atoms to their equilibrium values. A time step of integration of 2 fs was used in the Verlet algorithm in the CHARMM program (Brooks et al., 1983). No NMR restraints were used throughout the simulations. After the equilibration period of 200 ps, a production run of 1 ns constant energy molecular dynamics was completed with an average temperature of 300 K. Every 200 fs, coordinates and energetic data were collected. The core regions of the peptide, including the LVFFA and VGSN substructures, were largely similar in the four starting configurations. However, outside of that core structure, there was significant disorder in the N- and C-terminal regions of the peptide due to the small number of experimentally derived restraints in those regions that were used in the structural refinement.

Measures of peptide dynamics and reorganization

We use a number of useful measures of the peptide dynamics, including the rate of translational diffusion of the peptide and variations in the compactness of the peptide as measured by the radius of gyration and peptide end-to-end distance.

Self-diffusion constant for the peptide

The mean-square displacement of the center-of-mass of the peptide was computed as a function of time. The diffusion constant of the peptide monomer was estimated using the Einstein relation

$$\langle \Delta r_{COM}(t)^2 \rangle \sim 6Dt, \quad (1)$$

where $r_{COM}(t)$ is the center of mass coordinate. Eq. 1 is expected to hold in the limit of long times. The mean square displacement was computed over the length of the trajectory and the slope was measured to determine the diffusion constant.

Radius of gyration

The radius of gyration for the peptide was computed using all of the peptide atoms in the standard formula (Berne and Pecora, 1976)

$$r_g^2 = \sum_k^N m_k(r_k - r_{COM})^2 \bigg/ \sum_k^N m_k, \quad (2)$$

where r_k is the position of the kth atom in the peptide, and m_k is its mass. Summed averages were generated over each full trajectory to determine the ensemble averaged $\langle r_g^2 \rangle$.

Peptide end-to-end distance

The peptide's end-to-end distance was defined by the distance separating the first N atom of the N-terminal Tyr[10] and the second end N atom attached to the carbonyl carbon atom of the C-terminal Met[35]. That calculation is equivalent to the definition

$$r_e = \sum_i l_i, \quad (3)$$

where l_i is the vector connecting the consecutive N atoms along the backbone between the N- and C-termini. The ensemble averaged value $\langle r_e^2 \rangle$ was computed by averaging over the molecular dynamics trajectories. Large changes in r_e indicate significant reorganization in the peptide's global structure.

Characterizing the peptide structure in solution

For each saved configuration, the peptide was analyzed for hydrogen bonding groups for all possible donors and acceptors. The hydrogen bonding frequency was averaged over the full simulation by dividing the number of snapshots (instantaneous configurations) showing hydrogen bonds by the total number of snapshots. The following definition of the hydrogen bond was used: the donor and acceptor atoms were required to be at a distance shorter than or equal to 2.5 Å and the angle between the donor and acceptor diatomic groups is in the range 113–180° (Simmerling et al., 1995).

The atomic exposed surface area was computed by the method described by Wesson and Eisenberg (1992) and originally developed by Lee and Richards (1971). The solvent-exposed surface area of each atom was defined as the area exposed to contact by a water probe of diameter 2.8 Å. The upper bound on the solvent-exposed surface area was taken to be the surface area for the peptide in a modeled extended configuration. Each trajectory was analyzed by computing the total solvent-exposed surface area of the whole peptide (as well as a calculation restricted to those atoms composing the LVFFA region).

TABLE 1 The computed and experimentally derived values of the S^2 order parameter

	S^2		
Amino Acid	Simulation (WT)	Simulation (Dutch)	Experiment (WT)
Tyr[10]	0.21	0.01	
Glu[11]	0.50	0.32	
Val[12]	0.56	0.45	
His[13]	0.51	0.56	
His[14]	0.45	0.43	
Gln[15]	0.66	0.56	
Lys[16]	0.74	0.71	
Leu[17]	0.66	0.68	
Val[18]	**0.65**	**0.74**	**0.68 ± 0.05**
Phe[19]	**0.72**	**0.74**	**0.75 ± 0.05**
Phe[20]	**0.69**	**0.69**	**0.79 ± 0.05**
Ala[21]	0.51	0.47	
Glu[22]	0.66	0.52	
Asp[23]	0.51	0.48	
Val[24]	**0.55**	**0.58**	**0.75 ± 0.05**
Gly[25]	**0.66**	**0.55**	**0.76 ± 0.05**
Ser[26]	0.55	0.45	
Asn[27]	0.51	0.57	
Lys[28]	0.62	0.68	
Gly[29]	**0.55**	**0.70**	**0.64 ± 0.06**
Ala[30]	0.45	0.64	
Ile[31]	0.40	0.51	
Ile[32]	0.50	0.58	
Gly[33]	**0.43**	**0.45**	**0.54 ± 0.06**
Leu[34]	0.36	0.44	
Met[35]	0.41	0.43	

Lipari–Szabo NMR order parameters

We follow the standard "model free" analysis of Lipari and Szabo (1982a,b). The motion of the peptide can be described by a correlation function $C(t)$ for the orientation of a peptide backbone amide bond vector. Assuming that the internal motions are uncorrelated with the overall molecular tumbling, $C(t)$ can be factored into two contributions—one for the internal motions and another for the overall molecular rotation as

$$C(t) = C_{tumb}(t)C_{int}(t) = \frac{1}{5} e^{-t/\tau_0} C_{int}(t). \quad (4)$$

Using $Y_{2m}(\theta, \phi)$, the second-order spherical harmonics, with θ and ϕ specifying the orientation of the internuclear NH amide bond vector in the molecule-fixed coordinate frame, the internal motions of the peptide can be characterized by two parameters: a generalized order parameter, S,

$$S^2 = \lim_{t \to \infty} C_{int}(t) = \frac{4\pi}{5} \langle r^{-6} \rangle^{-1} \sum_{m=-2}^{2} \left| \left\langle \frac{Y_{2m}(\theta, \phi)}{r^3} \right\rangle \right|^2, \quad (5)$$

and an effective correlation time, τ_{int}.

S is a measure of the degree of freedom of the motion of the intermolecular amide bond vector; S is unity if the motion is completely restricted; S is zero for isotropic motion. To separate the overall molecular rotation from the internal motion, every coordinate frame of the 1-ns trajectory was translated and rotated until the root mean square (RMS) displacement with respect to a reference configuration ($t = 0$) was minimized (Philippopoulos and Lim, 1994). The values of the generalized order parameter, S^2, for the NH amide bond vector are presented in Table 1.
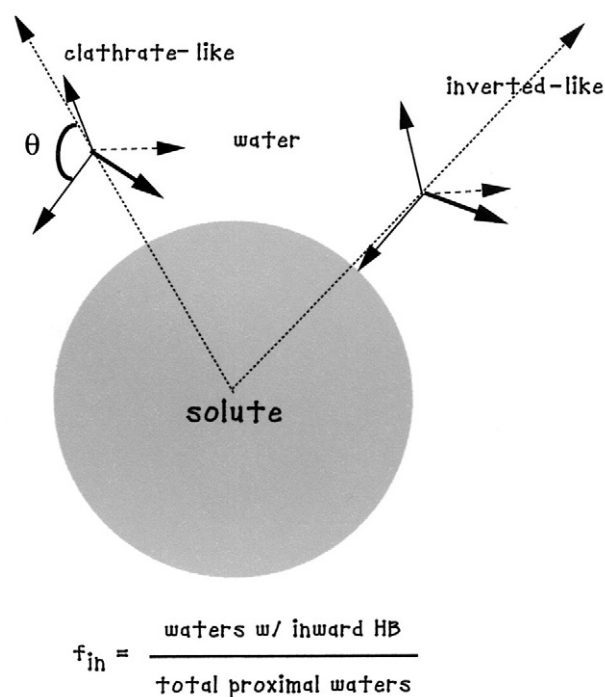
FIGURE 2 A schematic diagram describing the relation of the order parameter for the peptide's first hydration shell, after Fig. 2 of Cheng et al. (1999).

Cross correlation matrix analysis of peptide fluctuations

To develop a measure of the correlation in the fluctuations of the peptide residues, the cross correlation matrix of cartesian coordinate fluctuations was analyzed. The elements of the matrix are defined (Haliloglu and Bahar, 1998)

$$M_{ij} = \langle \Delta R_i \Delta R_j \rangle / \langle \Delta R_i^2 \Delta R_j^2 \rangle^{1/2}, \qquad (6)$$

where the angle brackets indicate an average over the length of the simulation. The correlation matrix is useful in recognizing groups of atoms that move with high correlation. This may be the case for clusters of atoms or residues as well as segments of secondary structure such as α-helices and β-sheets.

Peptide hydration analysis of the first solvation shell

Cheng and Rossky (1999) have proposed a novel measure of the hydration structure near a solute interface. It is known that water near the convex surface of a small hydrophobic solute tends to form a clathrate cage structure (Fig. 2). Such a solvation shell allows for water–water hydrogen bonding and reduces water–water hydrogen bonding enthalpy at the cost of decreasing the water's configurational entropy. Near a charged solute, the water molecules tend to assume an inverted orientation (Fig. 2) with an O–H bond or lone pair directed inward toward the solute.

However, when the hydrophobic solute–water interface is less convex, or even planar or concave, the water may no longer assume the classic clathrate cage structure, due to topological constraints. Cheng and Rossky have developed a number of measures of the degree of clathrate or inverted character in water orientation and applied those measures to examine the
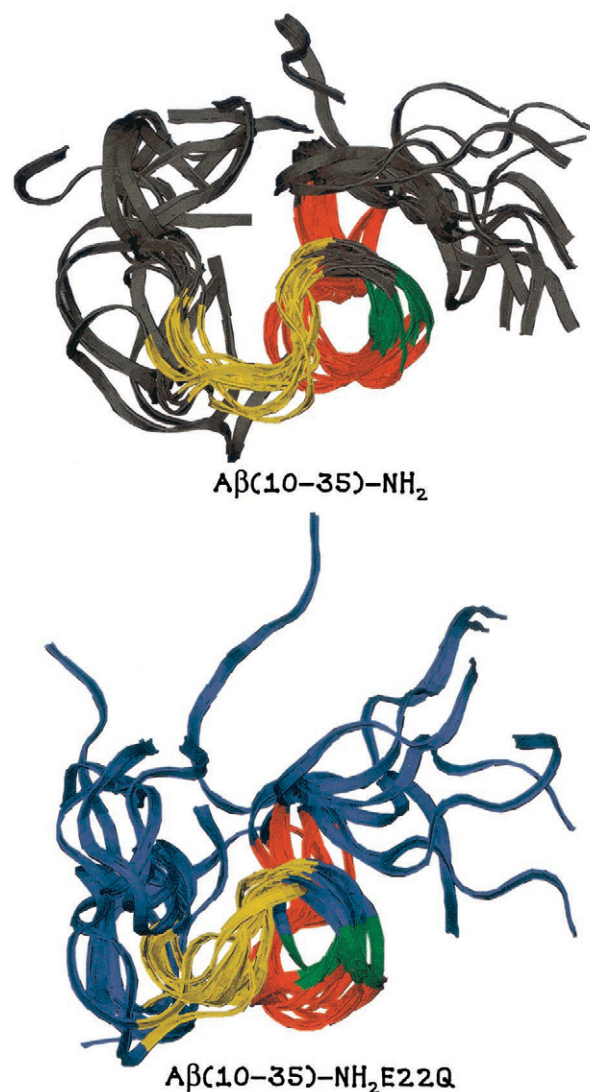

FIGURE 3 A collage composed of snapshot configurations taken every 100 ps along the four 1-ns trajectories for the WT or E22Q mutant peptide. The peptide backbone structures are overlapped to best fit the central core region of the peptide.

hydration shells of a number of proteins, including mellitin and the active site of α-chymotrypsin (Cheng and Rossky, 1999; Cheng et al., 1999; Carey et al., 2000). One of their measures is depicted in Fig. 2. The parameter f_{in} is an order parameter for the degree of clathrate-like or inverted water structure. Their analysis has shown that water structure near hydrophobic protein surfaces is sensitive to the topological constraints. In this work, we have used this measure to analyze the hydration structure over the full surface of the Aβ-peptide with a particular interest in the hydration structure in the region of the anomalously large hydrophobic patch centered about the LVFFA cluster. To further investigate the energetics of the hydration shells of the WT and mutant peptides, we also computed the average binding energy, E_b, of proximal water molecules for every residue of the peptide. The binding energy E_b was decomposed into contributions from the interaction of the water in the first solvation shell with all the other water molecules in the system, E_w, and with the peptide, E_p.
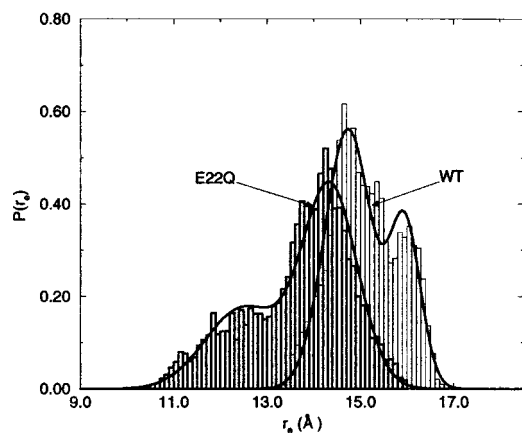
FIGURE 4   The end-to-end distance for the peptide computed for the simulation runs of both the WT and E22Q mutant peptides.

FIGURE 6   Plot of the amide bond vector order parameter S^2 for the simulation runs of both the WT and E22Q mutant peptides.

RESULTS

Peptide solution structure and fluctuations

The average structure and conformational fluctuations of the solvated WT and E22Q mutant peptides were determined from an analysis of the independent trajectories. The results were analyzed in terms of the average structure, the distributions of peptide end-to-end distance and radius of gyration, the fluctuations in the atomic positions and backbone torsional angles, and the computed amide bond vector orientational Lipari–Szabo order parameters.

WT and E22Q mutant peptide solution structures are similar

Overlapping instantaneous structures taken from the endpoints of the independent nanosecond trajectories are shown in Fig. 3. The core regions of the peptide, including the
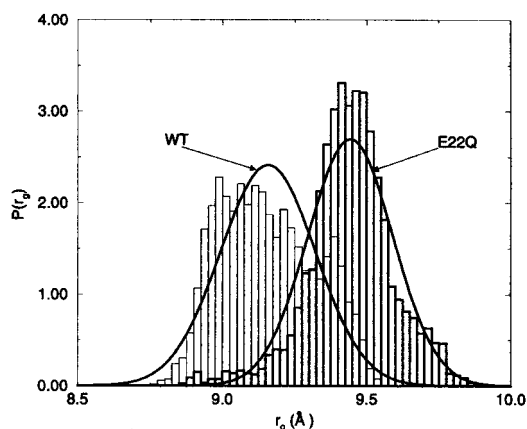
LVFFA central hydrophobic cluster and VGSN turn region, are largely conserved over the full length of the dynamics of the WT and E22Q mutant peptide. In both the WT and E22Q mutant peptides, the N-terminal region tends to be significantly more disordered than the C-terminal region. Overall, the average structures of the WT and E22Q mutant peptides are similar.

It has been reported that the monomeric E22Q mutant peptide assumes a β conformation in solution. However, our results indicate that the monomeric E22Q mutant peptide maintains a structure quite similar to the WT peptide over the length of our dynamical simulations.

Diffusion constants for WT and E22Q peptides are comparable

The translational self-diffusion constant for the E22Q mutant peptide was computed using the Einstein relation for

FIGURE 5   The radius of gyration of the peptide computed for the simulation runs of both the WT and E22Q mutant peptides.
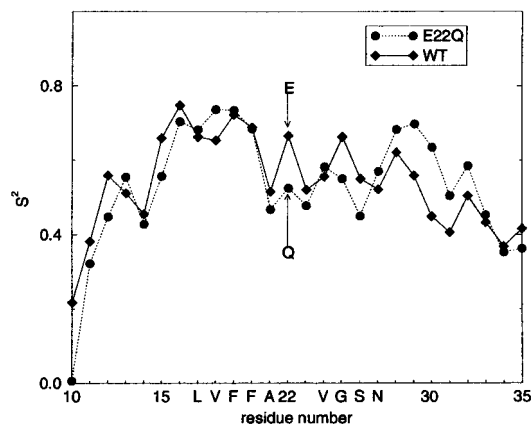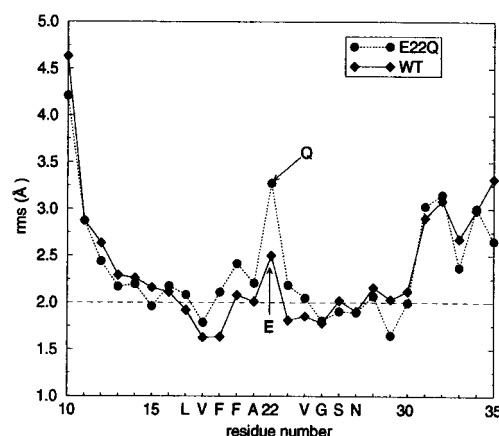

FIGURE 7   The averaged RMS atomic coordinate deviation from the average peptide structure computed over each of the simulation runs of both the WT and E22Q mutant peptides.
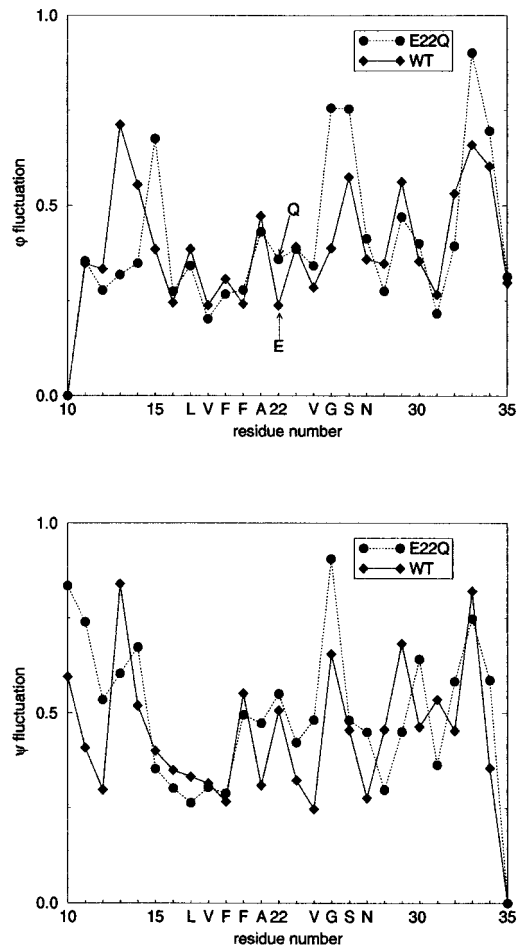
FIGURE 8 The averaged RMS atomic coordinate deviation from the average peptide structure computed for the ψ and ϕ backbone torsional angles for the simulation runs of both the WT and E22Q mutant peptides.
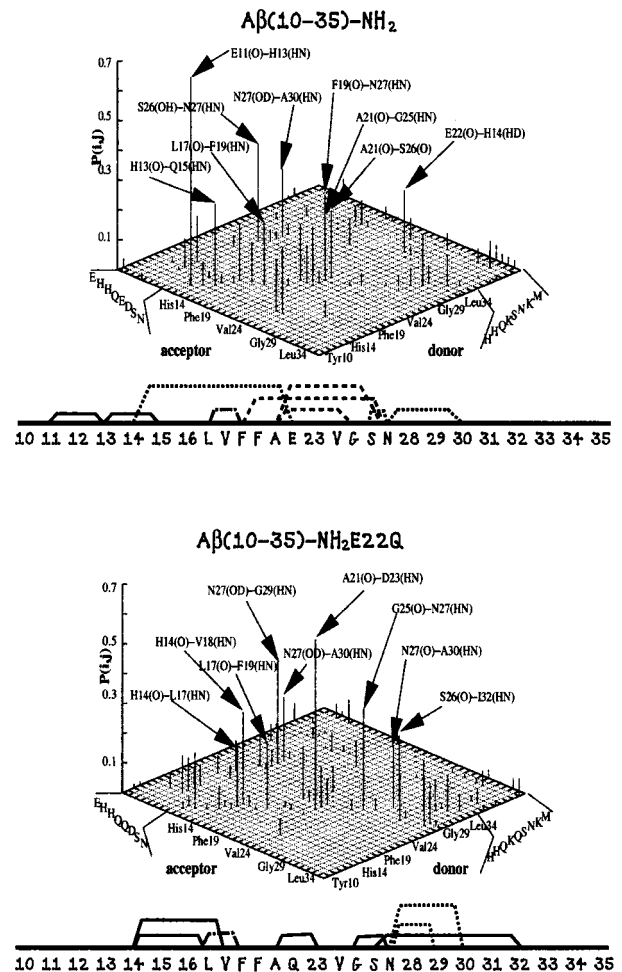

FIGURE 9 Plot of the hydrogen-bonding probabilities averaged for the simulations of the WT and E22Q mutant peptides. Hydrogen bond acceptors are noted along the x-axis and donors are indicated along the y-axis. The acceptors indicated with single letters are side chain groups; those that follow are backbone carbonyl oxygen atoms. Similarly, the donors indicated with single letters are side chain groups; the remaining donors are backbone amide hydrogen atoms. Below each histogram is found a plot depicting the connectivity of the most prominent hydrogen bonds. Connections are shown between the LVFFA and VGSN regions (*dashed*), between side chain and backbone groups (*dotted*), and between backbone and backbone groups (*solid*). Hydrogen bond connections found in common between the WT and E22Q mutant peptides are also noted (*dot-dashed*).

the mean-square displacement of the peptide's center of mass. Values of the diffusion constant were derived from fits to the asymptotic linear regions of the mean-square displacement. The average diffusion constant is approximately $D = (1.5 \pm 0.4) \times 10^{-6}$ cm^2/s. This is the same value, within the error, that was found from the simulation of the WT peptide, whose diffusion constant was estimated to be equal to $(1.4 \pm 0.4) \times 10^{-6}$ cm^2/s (Massi et al., 2001).

E22Q peptide end-to-end distance biased to short distances

The distributions of end-to-end distance, binned over the independent trajectories of the WT and E22Q mutant peptides, are depicted in Fig. 4. There is a significant difference in the distributions with the end-to-end distance in the E22Q mutant being significantly smaller, on

average, and broader, in fluctuation, than the distribution for the WT peptide.

E22Q peptide more open than WT

The distributions of the radius of gyration for the WT and E22Q mutant peptides are shown in Fig. 5. On average, the E22Q mutant peptide appears to be somewhat more expanded than the WT peptide. This is consistent with the

E22Q mutant peptide having a larger solvent-exposed surface area than is found for the WT peptide (see below).

Simulated NMR order parameters in WT and E22Q are similar

The NH amide bond vector Lipari–Szabo order parameters are plotted in Fig. 6. For the most part, the relative variation in the S^2 values, over the length of the peptide, is similar for each peptide. The N-terminal region is significantly more disordered than the C-terminal region in both the WT and E22Q mutant peptides. The LVFFA region has large amide bond vector orientational order in both peptides. There are, however, two distinct differences between the S^2 values of the WT and E22Q mutant peptides. The most notable difference is the significantly smaller S^2 value of residue 22 for the E22Q mutant peptide, indicating greater orientational fluctuation of the NH amide bond in the mutant peptide dynamics relative to the WT peptide. Also, in the 28–32 region of the peptide, the mutant peptide shows significantly greater correlation than in the corresponding region of the WT peptide.

There is a significantly greater average fluctuation of the atoms of residue 22 in the dynamics of the E22Q mutant peptide relative to the WT peptide (see Fig. 7). Large-scale motion of the N- and C-terminal regions is common to both peptides in all simulations. The central core regions of the peptide tend to show RMS fluctuations on the order of 2 Å. However, the RMS fluctuations of the Q22 residue in the E22Q mutant peptide appear to be on the order of 3 Å and comparable to the RMS fluctuations of atoms in the C-terminal region of the peptide. Note the large fluctuations in the loop region centered about residue Glu[22] in the dynamics of the mutant peptide. The larger fluctuations in Glu[22] are flanked by smaller fluctuations throughout the LVFFA (17–21) central hydrophobic cluster and particularly in the VGSN (24–27) turn region. The results are consistent with NMR measurements of the proton chemical shifts that demonstrate that these regions tend to be particularly well structured in aqueous solution and reasonably insensitive to changes in temperature in the range 5–35°C (Zhang, 1999).

The magnitude of fluctuations in the ϕ–ψ angles of the peptide's backbone are displayed in Fig. 8. The overall magnitude of fluctuations in the peptide's backbone is similar in the WT and E22Q mutant peptides. A difference can be seen in the VGSN region where the fluctuations appear to be significantly larger in the E22Q mutant peptide. Those larger fluctuations may be correlated with a somewhat diminished values of the S^2 order parameter in that region for the E22Q mutant peptide (see Fig. 6).
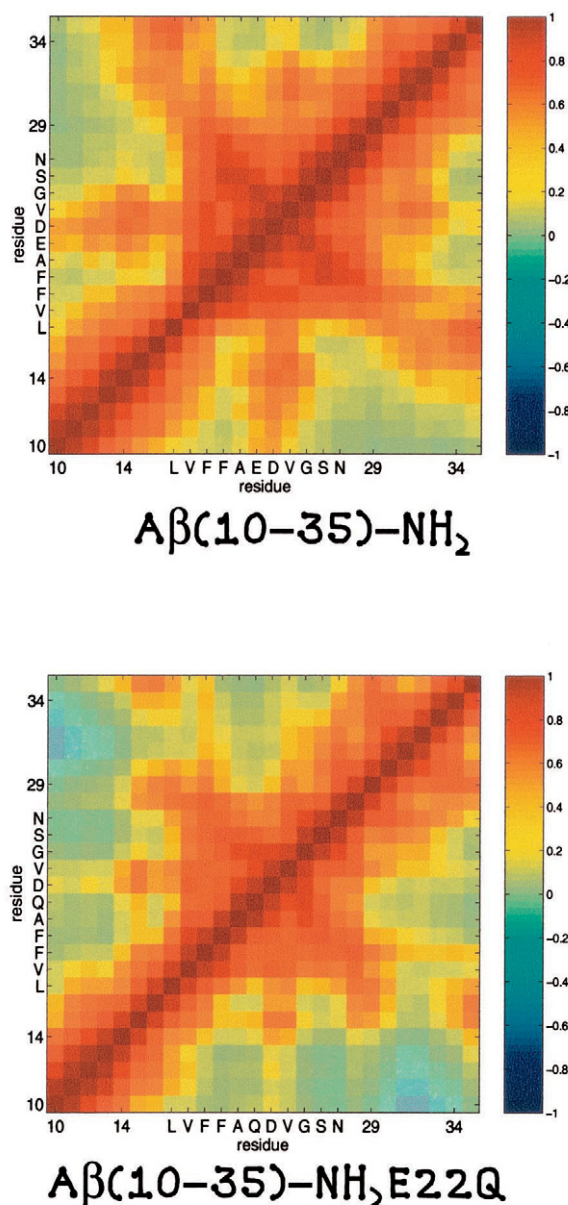

FIGURE 10 Averaged cross correlation of cartesian coordinate fluctuations in the residues of the WT and E22Q mutant peptides. Regions of red indicate strong correlation, and regions of blue indicate anticorrelation.

H-bonds between LVFFA and VGSN region disrupted in E22Q peptide

Although there are significant fluctuations in the structure of the WT and E22Q mutant peptide over the course of the nanosecond dynamical trajectories, the peptide has been shown to have a well-defined average structure in the central core region and within the fluctuating N- and C-terminal regions. The average structure is stabilized in part by clustering of nonpolar hydrophobic side chains and by the formation of hydrogen bonds.
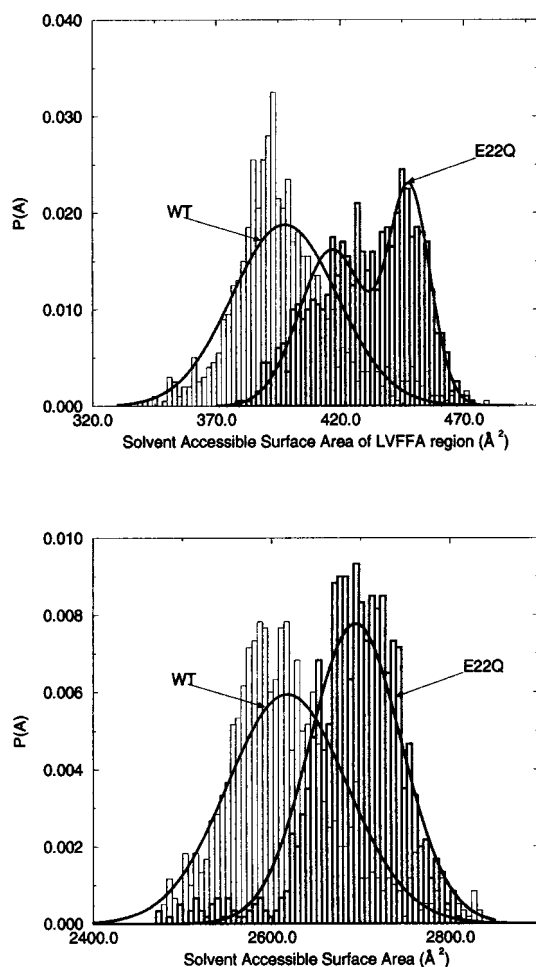
FIGURE 11 The atomic solvent-exposed surface area contributed by the central hydrophobic cluster LVFFA (*top*) and the total peptide (*bottom*) averaged over the simulations of the WT and E22Q mutant peptides.
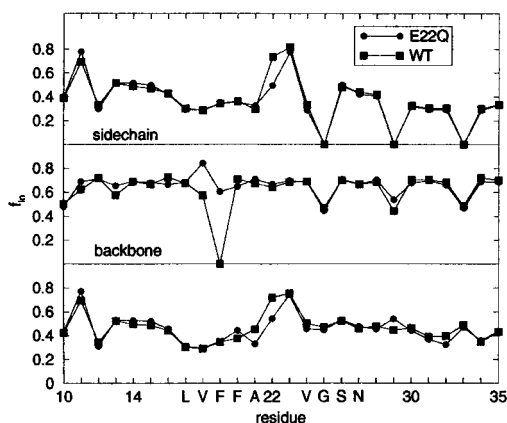

FIGURE 12 The time-averaged f_{in} order parameters for residues of the WT and E22Q mutant peptides. The separate averages over the atoms composing the side chains and backbone are also shown.

The frequency of observed hydrogen bonds is shown in Fig. 9 for both the WT and mutant E22Q peptides. The hydrogen bonds that occur with greatest frequency are labeled. Below each histogram is shown a summary of the prominent hydrogen bonds. There are several crucial differences and similarities in the hydrogen bonding patterns of the WT and E22Q mutant peptides.

The most striking difference between the hydrogen bonding patterns in the WT and E22Q mutant peptides is the connectivity between the LVFFA and VGSN regions in the WT peptide and the disruption of those hydrogen bonds in the E22Q mutant peptide. The E22Q point mutation is found at the interface between those two regions and it is sensible to assume that the larger structural fluctuations found at residue 22 in the E22Q mutant peptide (see above) are a result of the reduced stability of that region, resulting from the disruption of spanning hydrogen bonds between the residues of the LVFFA cluster and the VGSN turn regions. This is in agreement with experimental NMR amide hydrogen exchange-rate data, indicating that the average exchange lifetimes of residues 16–27, excluding V18 and V24, were reduced in the Aβ(12–28)E22Q mutant peptide relative to the wild type peptide (Zhang, 1999; Zhang et al., 1998). However, it should be noted that, in both trajectories, there are significant fluctuations, and none of the hydrogen bonds in either peptide are truly robust. The hydrogen bonds that do form tend to be formed intermittently.

The L17–F19 hydrogen bond is observed to be common to both the WT and E22Q mutant peptides. A second notable similarity is the apparent special role played by the N27 residue, which is a highly connected residue in both the WT and E22Q mutant dynamics. The statistics for each peptide show four different hydrogen-bond connections involving the N27 sidechain.

A significant difference in the observed hydrogen bonding patterns is that the N27 residue participates in two common hydrogen bonds between residues of the LVFFA region in the WT. However, in the E22Q mutant trajectories, N27 is connected by hydrogen bonds only to local turn residues or flanking residues in the C-terminal region.

Propensity for secondary structure fluctuations

It has been proposed that the difference in activity observed for the WT and E22Q mutant peptides can be attributed to a larger propensity for the formation of β structure in the monomeric E22Q mutant peptide in solution, relative to the WT peptide. To test this hypothesis, we have analyzed the cross correlation of residue fluctuations in the simulated peptide dynamics.

The computed cross correlation matrices are depicted in Fig. 10. A number of dominant features are apparent. There is a strong correlation of fluctuations in the residues of the peptide's core, including the LVFFA hydrophobic cluster
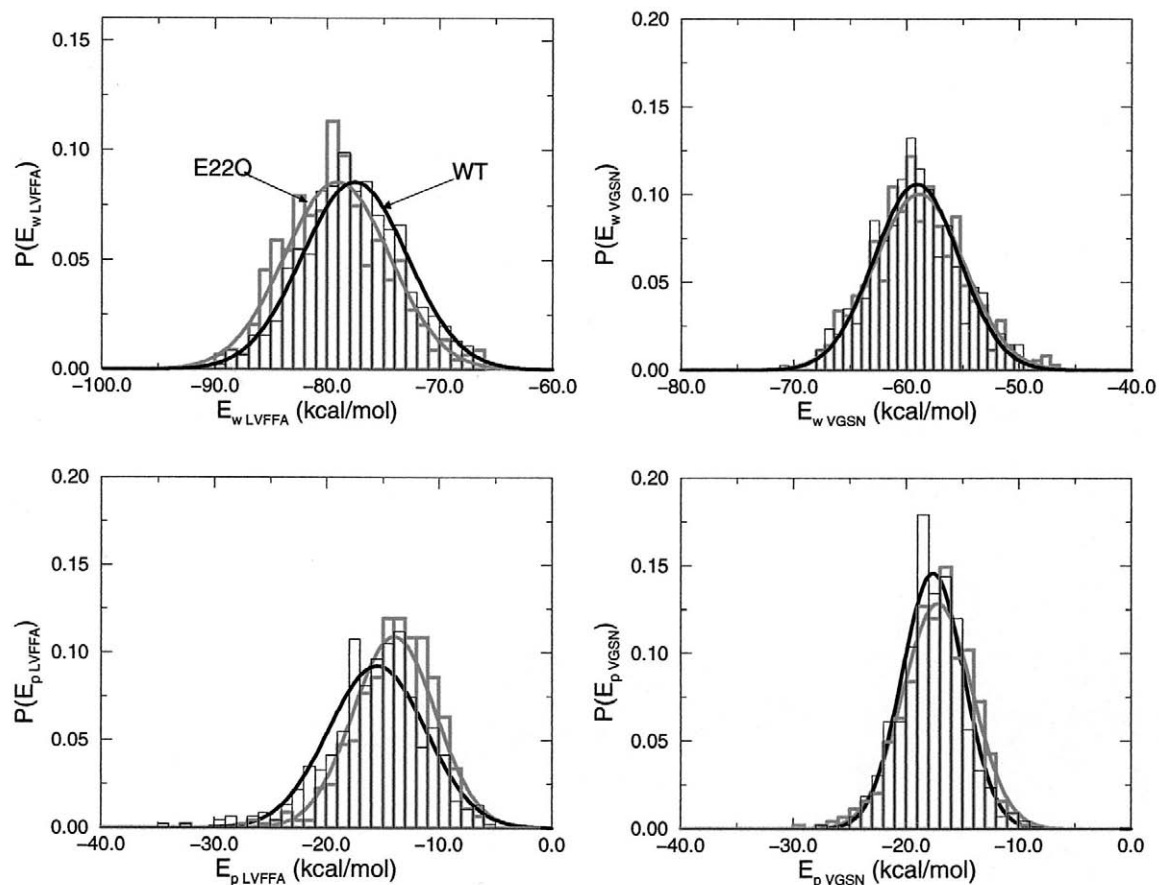
FIGURE 13 The average binding energy E_b for proximal water molecules, in the LVFFA region and in the VGSN region, is decomposed in the two contributions E_w (*top*) and E_p (*bottom*) over the simulation runs. The energy distributions corresponding to the E22Q mutant peptide are represented in gray, those of the WT in black.

FIGURE 14 The average binding energy E_b for proximal water molecules around residue 22 is decomposed in the two contributions E_w (*top*) and E_p (*bottom*) over the simulation runs. The energy distributions corresponding to the E22Q mutant peptide are represented in gray, those of the WT in black.
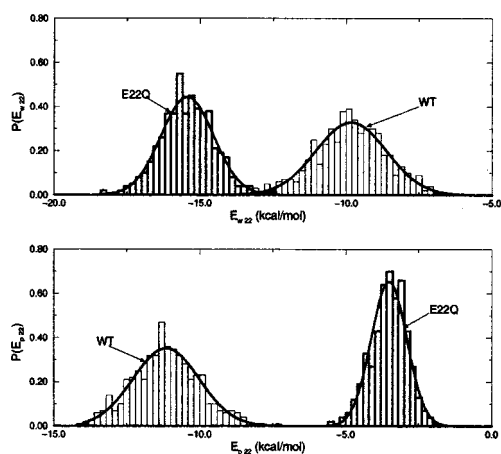
and VGSN turn regions. In the WT peptide, there is a large block of high correlation through the LVFFAEDVGSN (17–27) region of the peptide. In the E22Q mutant peptide, the correlation is noticeably weaker, in agreement with the observation that the hydrogen-bonding contacts between the LVFFA and VGSN regions are disrupted.

In both the WT and E22Q mutant data, there are shadows of the diagonal signature of antiparallel β-strand. This indicates the presence of correlated motion consistent with the formation of β-structure but in the absence of the formal hydrogen-bonding pattern of true β-sheet or strand (see above).

Peptide hydration

In the WT peptide, the E22 residue is negatively charged at neutral pH, whereas, in the E22Q mutant peptide, the Q22 residue is electrically neutral but polar. It is expected, therefore, that the difference could effect the peptide's activity in at least two ways. First, the desolvation step, which may occur at residue 22 in the aggregation of the peptide, could

be significantly different in the WT or E22Q mutant peptide. Furthermore, the charged E22 residue in the WT peptide would, presumably, become protonated or chelated with a cation if buried in an amyloid peptide aggregate.

E22Q structure is more solvent exposed than WT peptide

The distributions of total solvent-exposed peptide surface area and the solvent-exposed surface area contributed by the hydrophobic cluster of residues LVFFA (17–21) are displayed in Fig. 11. The E22Q mutant peptide shows a significantly larger absolute measure of solvent-exposed surface area contributed by the LVFFA cluster and over the full peptide.

The larger solvent-exposed surface observed for the E22Q mutant peptide (on average more than 100 Å^2) is consistent with the larger observed average radius of gyration of the E22Q mutant peptide relative to the WT peptide (on average 0.5 Å).

E22Q mutation leads to change in hydration of hydrophobic patch

We have examined the nature of the orientational order of the water in the first solvation shells of the WT and E22Q mutant peptides using the clathrate/inverted order parameter analysis developed by Cheng and Rossky (1999). The results for the averaged order parameter are plotted in Fig. 12.

The principal result of the mutation, from the polar Q22 residue in the Dutch mutant peptide to the charged E22 residue in the WT peptide, is the alteration of the local inverted water structure in the first solvation shell of residue 22. In both peptides, the LVFFA region is characterized by an f_{in} order parameter consistent with a somewhat clathrate-like solvation structure.

The result of the analysis of the energy of the water molecules in the first hydration shell of the LVFFA and VGSN regions is presented in Fig. 13. The binding energy, E_b, has been decomposed in the two contributions—the interaction energy of the water in the solvation shell with all the other water molecules in the system, E_w, and with the peptide, E_p. The distributions of E_w and E_p have been fit to gaussian distributions. The distributions of E_w show a different result for the LVFFA and the VGSN regions. The gaussian distribution for E_w of the LVFFA region of the E22Q mutant is shifted toward lower mean energy than that of the WT. The gaussian fit for E_w in the VGSN region does not differ significantly between the WT and E22Q peptides. A more negative value of E_w in the LVFFA region of the E22Q mutant relative to the WT peptide indicates that the structure of the water around this region is energetically more clathrate-like in the Dutch mutant than in the WT.

The distributions of E_p in the VGSN region are similar for the WT and the E22Q mutant peptides. In the LVFFA region, however, the distribution of E_p energies for the

E22Q mutant is characterized by higher energies relative to the same interactions in the WT peptide. This result demonstrates that the interaction between the water molecules in the first solvation shell of the LVFFA region of the peptide is less attractive in the Dutch mutant than in the WT.

The distributions of E_w and E_p for residue 22 are presented in Fig. 14. The distribution of the binding energy shows that the E22Q mutant peptide is characterized by more (favorable) negative values of E_w and less (favorable) negative values of E_p than in the WT peptide. The results can be explained by noting that the charged residue in the WT is expected to have a more attractive interaction with the solvent in an inverted structure. The mutation at residue 22 leads to a different structure and energy of the water around this residue, but also influences the fluctuations in the peptide and the structure and energetics of the first hydration shell about the LVFFA region.

When the monomeric peptide encounters a pre-existing fibril, there will be a desolvation step associated with the burial of the monomeric peptide's hydrophobic surface. In the case of the E22Q mutant, the desolvation step will be associated with an increase in solvent entropy and relatively little change in the solvent enthalpy. However, for the desolvation of the WT peptide, there will be a significant enthalpic cost associated with the desolvation of the charged E22 residue. Overall, the association of the monomeric peptide with the fibril interface is expected to be both enthalpically and entropically more favorable in the case of the E22Q mutant.

In a previous study (Esler et al., 2000a) it was suggested that different entropies of activation, $\Delta S^{\ddagger}$, characterize the aggregation process of the WT and E22Q mutant Aβ-peptides. That result was interpreted in terms of differing flexibility of the two peptides. In the light of our study, the different entropy of activation may be interpreted in terms of the solvation/desolvation process in the aggregation of the peptide. However, it is difficult to predict the exact effect that the changes in hydration shell structure have on the activation entropies of the peptides. The E22Q mutant peptide is characterized by a more clathrate-like structure of the first solvation shell, relative to the WT peptide, with a lower associated entropy. The difference between the relative conformational entropies of the peptides in solution is not so easily predicted, nor is the entropy difference of the transition states of the peptide–water system along the aggregation pathway. From our simulations of the peptides in aqueous solution, we cannot clearly predict either the value or the sign of the difference between the entropy of activation of the WT and E22Q mutant peptides for the aggregation process, $\Delta\Delta S^{\ddagger} = \Delta S^{\ddagger}_{WT} - \Delta S^{\ddagger}_{E22Q}$. Such an interpretation must await the results of a detailed analysis of proposed pathways for peptide aggregation currently under study (Massi and Straub, 2001).

SUMMARY AND CONCLUSIONS

The results of our multiple-nanosecond time scale molecular dynamics trajectories of the solvated $A\beta$ peptide congener in its WT and E22Q mutant forms support a number of conclusions related to the structure, fluctuations, dynamics, and hydration of the peptide.

1. The E22Q mutant and WT peptide are both stable in cc conformations consistent with the WT structure of Lee and coworkers (Zhang et al., 2000). The structure of the central hydrophobic core is preserved throughout the entire simulation for both systems.

2. In solution, the E22Q peptide is more flexible than the WT, supporting an early hypothesis that the equilibrium structural fluctuations of the E22Q mutant peptide were larger than those of the WT peptide (Zhang et al., 1998). The E22Q mutant peptide presents a wider distribution of the end-to-end distances than does the WT peptide. The fluctuations of the ϕ and ψ angles of the residues in the 22–27 region are larger in the E22Q mutant than in the WT peptide. The RMS fluctuations of atoms of the E22Q peptide are larger than those of the WT for all the aminoacids in the 17–26 region.

3. The values of the S^2 order parameter are consistently smaller in the Dutch mutant than in the WT peptide in the region between residue 21 and residue 26, which indicates that the motion of the NH amide bond is less restricted in the Dutch mutant than in the WT peptide. The absence of hydrogen bonds between the LVFFA and the VGSN regions in the E22Q mutant, which are present in the WT peptide, is correlated with the higher degree of flexibility of the structure of the mutant peptide around residue 22.

4. A comparison of the solvent-exposed surface area of the two peptides shows that the E22Q mutant peptide has a greater hydrophobic surface area exposed to the solvent. The mutant peptide also presents a larger radius of gyration than does the WT peptide. The local E22Q mutation leads to a local perturbation of the peptide hydration and the structure of the first solvation layer in the region of residue 22.

5. The water–water interaction energy for the waters of the first solvation shell of the LVFFA hydrophobic patch residues is significantly more favorable (more negative) in the mutant peptide. This is correlated with a less favorable (less negative) water–peptide interaction. Both observations are consistent with the formation of a more hydrophobic solvation shell over the hydrophobic patch of the E22Q mutant peptide. This difference should result in a small energetic cost of desolvation of the Dutch mutant peptide in the aggregation process relative to the WT peptide. These observations suggest that the Dutch mutant peptide may have a lower barrier and larger enthalpic driving force to desolvation and aggre-gation than does the WT peptide, in agreement with the noted increased activity of the Dutch mutant peptide.

REFERENCES

Berne, B. J., and R. Pecora. 1976. *Dynamic Light Scattering*. Wiley-Interscience, New York, NY. 169–171.

Brooks, B. R., R. Bruccoleri, B. Olafson, D. States, S. Swaninathan, and M. Karplus. 1983. CHARMM: a program for macromolecular energy minimization and dynamics calculations. *J. Comp. Chem.* 4:187–217.

Carey, C., Y. K. Cheng, and P. J. Rossky. 2000. Hydration structure of the alpha-chymotrypsin substrate binding pocket: the impact of constrained geometry. *Chem. Phys.* 258:415–425.

Cheng, Y. K., and P. J. Rossky. 1999. The effect of vicinal polar and charged groups on hydrophobic hydration. *Biopolymers.* 50:742–750.

Cheng, Y.-K., W.-S. Sheu, and P. J. Rossky. 1999. Hydrophobic hydration of amphipatic peptides. *Biophys. J.* 76:1734–1743.

Esler, W. P., A. M. Felix, E. R. Stimson, M. J. Lachenmann, J. R. Ghilardi, Y. Lu, H. V. Vinters, P. W. Mantyh, J. P. Lee, and J. E. Maggio. 2000a. Activation barriers to structural transition determine deposition rates of Alzheimer's disease $A\beta$ amyloid. *J. Struct. Biol.* 130:174–183.

Esler, W. P., E. R. Stimson, J. R. Ghilardi, H. V. Vinters, J. P. Lee, P. W. Mantyh, and J. E. Maggio. 1996. In vitro growth of Alzheimer's disease beta-amyloid plaques displays first-order kinetics. *Biochemistry.* 35: 749–757.

Esler, W. P., E. R. Stimson, J. M. Jennings, H. V. Vinters, J. R. Ghilardi, J. P. Lee, P. W. Mantyh, and J. E. Maggio. 2000b. Alzheimer's disease amyloid propagation by a template-dependent dock-lock mechanism. *Biochemistry.* 39:6288–6295.

Haliloglu, T., and I. Bahar. 1998. Coarse-grained simulations of conformational dynamics of proteins: application to apomyoglobin. *Proteins.* 31:271–281.

Kusumoto, Y., A. Lomakin, D. B. Teplow, and G. B. Bendek. 1998. Temperature dependence of amyloid β-protein fibrillization. *Proc. Natl. Acad. Sci. U.S.A.* 95:12277–12282.

Lee, B., and F. M. Richards. 1971. Interpretation of protein structures: estimation of static accessibility. *J. Mol. Bio.* 55:379–400.

Lee, J. P., E. R. Stimson, J. R. Ghilardi, P. W. Mantyh, Y.-A. Lu, A. M. Felix, W. Llanos, A. Behbin, M. Cummings, M. Van Criekinge, W. Timms, and J. E. Maggio. 1995. ^{1}H NMR of $A\beta$ amyloid peptide congeners in water solution. Conformational changes correlate with plaque competence. *Biochemistry.* 34:5191–5200.

Lipari, G., and A. Szabo. 1982a. Model free approach to the interpretation of nuclear magnetic resonance relaxation in macromolecules: 1. Theory and range of validity. *J. Am. Chem. Soc.* 104:4546–4559.

Lipari, G., and A. Szabo. 1982b. Model free approach to the interpretation of nuclear magnetic resonance relaxation in macromolecules: 1. Analysis of experimental results. *J. Am. Chem. Soc.* 104:4559–4570.

Mackerell, A. D. Jr., D. Bashford, M. Bellott, R. L. Dunbrack, Jr., J. D. Evanseck, M. J. Field, S. Fischer, J. Gao, H. Guo, S. Ha, D. Joseph-McCarthy, L. Kuchnir, K. Kuczera, F. T. K. Lau, C. Mattos, S. Michnick, T. Ngo, D. T. Nguyen, B. Prodhom, III, W. E. Reiher, B. Roux, M. Schlenkricha, J. C. Smith, R. Stote, J. Straub, M. Watanabe, J. Wiokiewicz-Kuczera, D. Yin, and M. Karplus. 1998. All-atom empirical potential for molecular modeling and dynamics studies of proteins. *J. Phys. Chem. B.* 102:3586–3616.

Marcinowski, K. J., H. Shao, E. L. Clancy, and M. G. Zagorski. 1998. Solution structure model of residues 1–28 of the amyloid β-peptide when bound to micelles. *J. Am. Chem. Soc.* 120:11082–11091.

Massi, F., J. W. Peng, J. P. Lee, and J. E. Straub. 2001. Simulation study of the structure and dynamics of the Alzheimer's amyloid peptide congener in solution. *Biophys. J.* 80:31–44.

Massi, F., and J. E. Straub. 2001. Energy landscape theory for Alzheimer's amyloid β-peptide fibril elongation. *Proteins.* 42:217–229.

Melchor, J. P., L. McVoy, and W. E. Van Nostrand. 2000. Charge alterations of E22 enhance the pathogenic properties of the amyloid β-protein. *J. Neurochem.* 74:2209–2212.

Miravalle, L., T. Tokuda, R. Chiarle, G. Giaccone, O. Bugiani, F. Ragliavini, B. Frangione, and J. Ghiso. 2000. Substitutions at codon 22 of Alzheimer's Aβ peptide induce diverse conformational changes and apoptotic effects in human cerebral endothelial cells. *J. Biol. Chem.* 275:27110–27116.

Philippopoulos, M., and C. Lim. 1994. Internal motions in the molecular tumbling regime. Effect on NMR dipolar cross relaxation and interproton distance determination. *J. Phys. Chem.* 98:8264–8273.

Selkoe, D. J. 1997. Alzheimer's disease: genotypes, phenotypes, and treatments. *Science.* 275:630–631.

Selkoe, D. J. 1994. Alzheimer's disease: a central role for amyloid. *J. Neuropath. Exp. Neurol.* 53:438–447.

Shao, H., J. Shu-chuang, K. Ma, and M. G. Zagorski. 1998. Solution structure of micelle-bound amyoid β (1–40) and (1–42) peptides of Alzheimer's disease. *J. Mol. Biol.* 285:755–773.

Sian, A. K., E. R. Frears, O. A. El-Agnaf, B. P. Patel, M. F. Manca, G. Siligardi, R. Hussain, and B. M. Austen. 2000. Oligomerization of β-amyloid of the Alzheimer's and the dutch-cerebral-haemorrhage. *Biochem. J.* 349:299–308.

Simmerling, C., R. Elber, and J. Zhang. 1995. A program for visualization of structure and dynamics of biomolecules and STO—a program for computing stochastic paths. In *Modelling of Biomolecular Structure and Mechanisms.* A. Pullman et al. (eds.), Kluwer, Netherlands. 241–265.

Talafous J., K. J. Marcinowski, G. Klopman, and M. G. Zagorski. 1994. Solution structure of residues 1–28 of the amyloid β-peptide. *Biochemistry.* 33:7788–7796.

Watson, D. J., A. D. Landers, and D. J. Selkoe. 1997. Heparin-binding properties of the amyloidogenic peptides Aβ and amylin. *J. Biol. Chem.* 272:31617–31624.

Wesson, L., and D. Eisenberg. 1992. Atomic solvation parameters applied to molecular dynamics of proteins in solution. *Protein Sci.* 1:227–235.

Zagorski, M. G., and C. J. Barrow. 1992. NMR studies of amyloid β-peptides: proton assignments, secondary structure, and mechanism of an α-helix→β-sheet conversion for a homologous, 28-residue, N-terminal fragment. *Biochemistry.* 31:5621–5631.

Zhang, S. 1999. Studies of β amyloid congeners directed toward understanding the mechanism underlying the formation of amyloid deposits in Alzheimer's disease. Ph.D. Thesis, Boston University, Boston, MA.

Zhang, S., K. Iwata, M. J. Lachenman, J. W. Peng, S. Li, E. R. Stimson, Y. A. Lu, A. M. Felix, J. E. Maggio, and J. P. Lee. 2000. The Alzheimer's peptide Aβ peptide adopts a collapsed coil structure in water. *J. Struct. Biol.* 130:130–141.

Zhang, S. S., N. Casey, and J. P. Lee. 1998. Residual structure in the Alzheimer's disease peptide: probing the origin of a central hydrophobic cluster. *Fold. Desg.* 3:413–422.